Predictor-Corrector Entry Guidance for Low-Lifting Vehicles

Ping Lu*

Iowa State University, Ames, Iowa 50011-2271

This paper investigates a numerical predictor-corrector methodology for adaptive and accurate entry guidance for vehicles with low lift-to-drag ratios, such as the Orion Crew Exploration Vehicle. The central ingredient in this approach is bank-angle parameterization. The choice of the bank-angle profile representation determines how the guidance problem will be solved, as well as the efficiency, performance, and robustness of the algorithm. Two popular forms of bank-angle parameterization, one in longitudinal mode and the other in three-dimensional mode, are closely examined. Special new robustification features are designed in the bank-angle parameterization that are shown to noticeably increase the overall performance of the algorithm. With the use of the predictor-corrector entry guidance approach, an interesting characteristic of the entry trajectory of a low-lifting vehicle is identified that reveals a definitive trend between the initial bank-angle magnitude and the peak load factor. Based on this observation, a simple and effective predictive load-relief strategy is developed for low-lifting vehicles. Extensive dispersion simulations are conducted to evaluate and verify the design features of the algorithm. The testing shows that the robustified longitudinal mode of the predictor-corrector entry guidance algorithm consistently offers very satisfactory performance even in highly dispersed cases. Such an algorithm holds distinct potential for onboard applications.

Nomenclature

e	=	nondimensional (negative) specific energy, $e = 1/r - V^2/2$
g_0	=	gravitational acceleration at R_0, 9.81 m/s^2
L, D	=	nondimensional aerodynamic lift and drag accelerations, g
n_a	=	aerodynamic load factor, g, $n_a = \sqrt{L^2 + D^2}$
R_0	=	radius of the Earth, 6,378,135 m
r	=	radial distance from the Earth's center to the vehicle, normalized by R_0
s	=	great-circle range to go, normalized by R_0
V	=	Earth-relative velocity, normalized by $\sqrt{g_0 R_0}$
γ	=	Earth-relative flight-path angle, rad
θ, ϕ	=	longitude and latitude, rad
ρ	=	atmospheric density, kg/m^3
σ	=	bank angle, rad
τ	=	time, normalized by $\sqrt{R_0/g_0}$
ψ	=	Earth-relative heading angle, rad, measured from north in clockwise direction
Ω	=	self-rotation rate of the Earth, normalized by $\sqrt{g_0/R_0}$

I. Introduction

PREDICTOR-CORRECTOR entry guidance algorithms have long been used in mission analyses and simulations for feasibility and trade studies of various entry vehicles and aerobraking missions. References [1–7] represent just a small chronological sampling of the relevant literature, and they are chosen to reflect the diversity of the applications. The common traits among this class of methods are the numerical or analytical propagation of the trajectory for the prediction of the final condition and the correctional steps to adjust the design parameters to null the errors in meeting the terminal constraints. The differences lie in the problem parameterization,

numerical or analytical procedures, and the details of the implementation. The predictor-corrector method enables the guidance system to design the entry trajectory and guide the vehicle adaptively without the need to rely on a prestored trajectory. This capability could give greater flexibility for the vehicle to handle larger dispersions and accommodate more severe off-nominal conditions. In addition, the generation of guidance commands would no longer rely on tracking the prespecified reference trajectory, a task that is made significantly more difficult by the lack of good maneuverability of low-lifting vehicles.

The Orion Crew Exploration Vehicle (CEV) will be a capsule vehicle. For entry vehicles such as the CEV or Apollo Command Module, the lift-to-drag (L/D) ratios are quite low, typically about 0.3 or even lower. For this class of vehicles, the shuttle entry guidance approach [8] is not applicable in flight regimes approximately below Mach 4, mainly due to the violations of certain underlying assumptions used in deriving the shuttle entry guidance principles (e.g., small flight-path angle). On the other hand, the Apollo final-phase entry guidance [9] guides the vehicle to follow a prestored longitudinal profile. The guidance law is linear, and the time-varying guidance gains are generated by the adjoint method based on the linearized trajectory dynamics. The low-lifting capability of capsule-type vehicles inherently constrains the ability to track a specified trajectory in the presence of large dispersions. The linearization approximation could further limit how far the actual trajectory can deviate from the reference. There are, indeed, potential cases in the anticipated mission scenarios of the Orion CEV in which the trajectory dispersions can be significant, such as in an anytime lunar-return mission or aborts.

The class of numerical predictor-corrector entry guidance methods has been under investigation since the 1980s. The essence of all reported approaches is to search for a bank-angle profile online to meet the mission objectives. The design philosophy is to keep the number of search parameters at a minimum for the simplicity and efficiency of the algorithm for onboard applications. Under these guidelines, there are two prevalent ways of parameterizing the bank-angle profile and solving the problem. One way is to search for just the magnitude of the bank-angle profile [2,3,6,7]. The sign of the bank-angle command is determined separately by another logic, such as the Apollo-type of bank-reversal logic [9]. Because the magnitude of the bank angle only defines the longitudinal motion of the vehicle through the trajectory dynamics, this approach is called the longitudinal mode in this paper. The simplest form in longitudinal mode is one that parameterizes a constant bank-angle magnitude

*Professor, Department of Aerospace Engineering, 2271 Howe Hall; plu@iastate.edu. Associate Fellow AIAA.

with one search parameter. An exception is Zimmerman et al. [6], in which a two-parameter profile is used to define the bank-angle magnitude profile. The choice of one more parameter in Zimmerman et al. is necessitated by an additional terminal constraint on the heading angle for a winged vehicle.

Another way is to find a complete bank-angle profile (including the magnitude and sign) [4,5], which will require a minimum of two search parameters. Once a complete bank-angle profile is defined, so is the complete three-dimensional entry trajectory for given initial condition, assuming that the vehicle flies at a trim angle of attack as is the case for capsule vehicles. Hence, this formulation will be called the 3-D mode.

The first objective of this paper is to investigate enhancements to both the existing longitudinal and 3-D modes of the predictor-corrector method aimed at entry guidance applications for vehicles with low L/D ratios. Chief among them is a robustifying feature we designed in the parameterization of the bank-angle magnitude, which allows a sufficient energy margin to be reserved toward the end of the trajectory while keeping the minimum number of search parameters. This feature affords our algorithm markedly more robust guidance performance with respect to large trajectory dispersions and modeling uncertainties than the existing approaches. Stressful dispersion testing proves that this unique design is indispensable for the predictor-corrector algorithm to meet the stringent landing precision requirement in the current Orion CEV program.

For a crewed vehicle such as the Orion CEV, the aerodynamic load factor along the entry trajectory is an important consideration in choosing the entry condition and evaluating the guidance performance. Various load-relief measures have been proposed in the entry guidance logic [2,9]. They are all reactive in nature in that the guidance system reacts by lifting up when the load factor exceeds the threshold. But the inherent limitation in the lifting capability of a vehicle with a low L/D renders such load-relief measures less effective and, in some cases, adversely affects the landing precision greatly. In this paper, we show that the bank angle used during the initial descent in the entry flight has an appreciable effect on the subsequent peak load factor. Based on this finding, an effective *predictive* load-relief strategy is developed that takes advantage of the trajectory prediction capability of the predictor-corrector algorithm. An appropriate bank angle during this initial descent phase is determined based on the predicted peak load factor in the subsequent trajectory, so as to keep the peak load factor below the required level while the landing precision is still ensured.

The final objective of this work is to evaluate and compare the longitudinal and 3-D modes of the predictor-corrector method and, if possible, identify the clear candidate for entry guidance applications. To this end, extensive 3-degree-of-freedom dispersion simulations are performed. The testing shows with compelling evidence that the design features, from the enhanced robustness to the predictive load-relief strategy, help achieve the intended effects. The robustified longitudinal mode of the algorithm demonstrates very strong robustness with respect to the vehicle modeling and environmental uncertainties and scores a success rate of 99.95% and above in all of the tests, even after the aerodynamic uncertainty is doubled. The predictive load-relief measure effectively reduces the peak load factor markedly on the dispersed trajectories without compromising the guidance precision. However, despite the enhancements in this work, we find through stressful dispersion testing that the 3-D mode of the predictor-corrector algorithm renders a less than stellar performance compared with the robustified longitudinal mode. We will provide a discussion on the reason why, which will shed some insightful light on good entry trajectory design.

II. Formulation of the Problem

The dimensionless 3-DOF equations of motion of an entry vehicle over a spherical, rotating Earth are given by

$$\dot{r} = V \sin \gamma \qquad (1)$$

$$\dot{\theta} = \frac{V \cos \gamma \sin \psi}{r \cos \phi} \qquad (2)$$

$$\dot{\phi} = \frac{V \cos \gamma \cos \psi}{r} \qquad (3)$$

$$\dot{V} = -D - \left(\frac{\sin \gamma}{r^2}\right) + \Omega^2 r \cos \phi (\sin \gamma \cos \phi - \cos \gamma \sin \phi \cos \psi) \qquad (4)$$

$$\dot{\gamma} = \frac{1}{V} \left[L \cos \sigma + \left(V^2 - \frac{1}{r}\right)\left(\frac{\cos \gamma}{r}\right) + 2\Omega V \cos \phi \sin \psi \right. $$
$$\left. + \Omega^2 r \cos \phi (\cos \gamma \cos \phi + \sin \gamma \cos \psi \sin \phi) \right] \qquad (5)$$

$$\dot{\psi} = \frac{1}{V} \left[\frac{L \sin \sigma}{\cos \gamma} + \frac{V^2}{r} \cos \gamma \sin \psi \tan \phi \right. $$
$$\left. - 2\Omega V (\tan \gamma \cos \psi \cos \phi - \sin \phi) + \frac{\Omega^2 r}{\cos \gamma} \sin \psi \sin \phi \cos \phi \right] \qquad (6)$$

where the differentiations are with respect to the dimensionless time τ. Because the time is not a critical parameter in entry flight, we will use an energylike variable e as the independent variable:

$$e = \frac{1}{r} - \frac{V^2}{2} \qquad (7)$$

It is clear that e as defined is the negative of the specific mechanical energy used in orbital mechanics. If the Earth-rotation term in Eq. (4) is ignored, it can be readily shown that

$$\frac{\mathrm{d}e}{\mathrm{d}\tau} = DV > 0 \qquad (8)$$

Therefore, e is a monotonically increasing variable. Let $\boldsymbol{x} = (r \quad \theta \quad \phi \quad \gamma \quad \psi)^T$ be the independent state vector, whereas the velocity V is determined by the values e and r from Eq. (7). The full 3-DOF equations of motion (1–6), excluding Eq. (4), may be rewritten with e as the independent variable:

$$\boldsymbol{x}' = \frac{\mathrm{d}\boldsymbol{x}}{\mathrm{d}e} = \boldsymbol{f}(\boldsymbol{x}, \sigma) \qquad (9)$$

It should be noted that the trim angle of attack profile the vehicle flies is assumed to be a given function of Mach number, and this dependence is already included in Eq. (9). The initial condition of the system (9) is taken to be the current state $\boldsymbol{x}_0$ at the current energy e_0. The final constraint is that the trajectory reaches the coordinates (Θ^*, Φ^*) of the target location at a specified final energy e_f.

$$\boldsymbol{x}(e_0) = \boldsymbol{x}_0 \qquad (10)$$

$$\theta(e_f) = \Theta^*, \quad \phi(e_f) = \Phi^* \qquad (11)$$

Alternative conditions equivalent to the two constraints in Eq. (11) can be written in terms of the final downrange $d(e_f)$ and cross range $\chi(e_f)$:

$$d(e_f) = 0, \qquad \chi(e_f) = 0 \qquad (12)$$

The problem of planning a feasible trajectory is to find the bank-angle profile so that the corresponding trajectory of the system equations (9) will satisfy the boundary conditions (10) and (11) [or

Eq. (12)]. Note that no optimization index of any kind is explicitly stated in the problem formulation. When this problem is repeatedly solved onboard, always with the current condition as the initial condition, and the guidance command applied is the value of the obtained bank-angle profile at the current instant, this process constitutes in effect closed-loop entry guidance. The focus of this paper lies in how the bank-angle profile may be parameterized so that this task can be rapidly accomplished and the possible onboard applications can be examined.

What is not explicitly stated in the aforementioned problem formulation is any inequality trajectory constraints. This is not an oversight. Vehicles with low L/D ratios have a very limited capability to significantly reshape the entry trajectory once the flight condition is given at a point of sufficient dynamic pressure. Imposing the inequality trajectory constraints in the guidance solution beyond any minor level would make the solution process overly complicated, yet still with rather limited effectiveness. Oftentimes, the landing precision will suffer markedly as a consequence of the interruption in the steering guidance. Therefore, for low-lifting entry vehicles, a more effective approach to rein in the inequality trajectory constraints, such as those on the load factor or heating rate, is to affect the condition at the point where the vehicle enters the dense atmosphere. This line of thinking is reflected in Sec. V, in which the load-factor constraint is addressed.

III. Longitudinal Mode

In this longitudinal mode, a one-parameter profile is sought online to determine the magnitude of the bank angle based on the current condition. The requirement that defines the bank-angle magnitude profile is that the total range flown from the current point to the given final energy is equal to the current range to go to the landing site.

A. Baseline Algorithm

Let s denote the range to go along the great circle connecting the current location of the vehicle and the landing site. It can be shown that the differential equation for s is

$$\dot{s} = -\frac{V \cos \gamma}{r} \tag{13}$$

Also notice from the equations of motion, Eqs. (1–6), that the longitudinal motion involving r, V, and γ is decoupled from the lateral motion variables, when the Earth's rotational effects are ignored. Therefore, the longitudinal motion with $\Omega = 0$ may be represented by the system

$$\dot{s} = -\frac{V \cos \gamma}{r} \tag{14}$$

$$\dot{r} = V \sin \gamma \tag{15}$$

$$\dot{V} = -D - \left(\frac{\sin \gamma}{r^2}\right) \tag{16}$$

$$\dot{\gamma} = \frac{1}{V}\left[L \cos \sigma + \left(V^2 - \frac{1}{r}\right)\left(\frac{\cos \gamma}{r}\right)\right] \tag{17}$$

Again, eliminating the equation for V by using the specific energy e in Eq. (7) as the independent variable, we have the three longitudinal equations

$$\frac{\mathrm{d}s}{\mathrm{d}e} = -\frac{\cos \gamma}{rD} \tag{18}$$

$$\frac{\mathrm{d}r}{\mathrm{d}e} = \frac{\sin \gamma}{D} \tag{19}$$

$$\frac{\mathrm{d}\gamma}{\mathrm{d}e} = \frac{1}{DV^2}\left[L \cos \sigma + \left(V^2 - \frac{1}{r}\right)\left(\frac{\cos \gamma}{r}\right)\right] \tag{20}$$

where $V = \sqrt{2(1/r - e)}$. Set the initial values of the state variables to be the current condition based on the navigation data (in particular, the initial value of $s(e_0)$ is equal to the current range to go to the landing site). For a given magnitude profile of the bank angle σ, the integration of these equations from the current condition to the specified final energy e_f gives the final range to go $s(e_f)$. A positive value of $s(e_f)$ indicates an undershoot, and a negative $s(e_f)$ means an overshoot of the landing site. The terminal constraint on the longitudinal motion is then

$$s_f = s(e_f) = 0 \tag{21}$$

The longitudinal predictor-corrector guidance problem can now be formulated in principle as follows: in each guidance update cycle, a constant σ is to be found so that the longitudinal trajectory leading from the current condition to the final energy e_f satisfies the constraint (21). Through the integration of the governing equations (18–20), the final range to go s_f can be regarded as a function of σ. The Newton–Raphson algorithm works as well for this one-parameter problem. With the Newton–Raphson method, the iterates on σ are given by

$$\sigma^{(k+1)} = \sigma^{(k)} - \frac{s_f(\sigma^{(k)})}{\partial s_f(\sigma^{(k)})/\partial \sigma} \tag{22}$$

where the partial derivative $\partial s_f(\sigma^{(k)})/\partial \sigma$ is obtained by a finite difference approximation.

In this process of the longitudinal mode, the sign of the bank angle is immaterial because only $\cos \sigma$ is involved in the longitudinal dynamics equations (18–20). When this mode is applied for guidance purposes, the appropriate sign of the bank angle will be required. The initial sign of the bank angle is chosen to be the opposite of the sign of the initial cross range. Then the sign of the bank angle is reversed whenever the cross range exceeds the velocity-dependent deadband [9], whose width y is defined by

$$y = c_1 V + c_0 \tag{23}$$

where c_1 and c_0 are the two constants. This Apollo-like lateral logic regulates the cross range to ensure a flight direction toward the landing site. The lifting capability, size, and weight of a vehicle determine how quickly it can change its flight direction, and unnecessary bank reversals could prematurely deplete the propellant of the reaction control system. Therefore, the constant equation (23) may need to be tuned for different vehicles for a good balance between cross-range regulation tightness and reasonable number of bank reversals.

B. Robustification and Further Modification

The aforementioned predictor-corrector algorithm computes a longitudinal trajectory that depletes all of the excess energy as soon as the range to go reaches zero. But the rate of the energy dissipation is not a design consideration. It could happen that in some cases the trajectory depletes much of its energy in the first half of the flight and leaves a relatively little energy margin in the second half, just the minimum amount to get to the landing site according to the nominal dynamic and environment models. This is not desirable from a practical viewpoint, because aerodynamic modeling uncertainties and atmospheric dispersions could render the vehicle short of energy toward the end of the trajectory.

A good measure of the energy margin along the entry trajectory is the magnitude of the bank angle. A magnitude of 60 deg in bank angle indicates that the vehicle only needs half of its lifting capability to maintain the longitudinal flight (because $\cos(60 \text{ deg}) = 0.5$). On the other hand, a bank angle with a small magnitude means that the vehicle is flying with nearly full lift up, and there is little margin left to

accommodate any further need to loft the trajectory. Without increasing the complexity of the algorithm, the parameterization of the bank-angle magnitude in the longitudinal predictor-corrector approach can be constructed to reserve a sufficient energy margin toward the end of the trajectory. One simple way is to specify a final magnitude of the bank angle, say, at $\sigma_f = 60$–70 deg. The single parameter that is sought by the algorithm to define the bank-angle magnitude profile is $\sigma_0 \geq 0$, the bank angle at the current energy e_0. The two parameters σ_0 and σ_f then determine a linear bank-angle magnitude profile:

$$|\sigma| = \sigma_0 + \frac{(\sigma_f - \sigma_0)}{(e_f - e_0)}(e - e_0), \qquad \sigma_f = 70 \ \text{deg} \qquad (24)$$

This bank-angle profile is used in the integration of the equations in Eqs. (18–20) to evaluate the final range to go s_f. Hence, s_f is a function of the free parameter σ_0. The same predictor-corrector algorithm outlined in the preceding section will be employed to find σ_0 such that $s_f(\sigma_0) = 0$. This simple measure is found to markedly improve the robustness of the algorithm (see Sec. VI).

Another modification to the baseline longitudinal mode is to use the full 3-DOF dynamics (1–6) in place of the reduced longitudinal dynamics in Eqs. (14–17). In this case, the sign of the bank angle along the predicted trajectory will be required in the predictor-corrector algorithm, in addition to the magnitude defined by Eq. (24). The sign is determined by the bank-reversal logic described at the end of Sec. III.A (albeit instantaneous bank reversals inside the trajectory integration). Although it has little effect on the accuracy of the algorithm in terms of landing precision, this seemingly minor modification has a noticeable effect on the peak aerodynamic load along the trajectory. A trajectory under the longitudinal predictor-corrector guidance with this modification tends to have a lower peak load factor than with reduced dynamics in Eqs. (15–17); the peak load factor along the predicted trajectory is a more accurate estimate to the actual one. This feature will prove advantageous in the predictive load-relief strategy to be discussed in Sec. V. The chief reason for these differences lies in whether or not the effects of the Earth's rotation are included in the trajectory prediction. In particular, the Earth's rotation has a nontrivial influence on the flight-path angle dynamics in Eq. (5) at the beginning of the entry flight where the gravity and centrifugal forces nearly balance each other ($V^2 \approx 1/r$) and the aerodynamic lift is negligible ($L \approx 0$). Ignoring this effect as in Eq. (17) is the main source of these differences.

IV. Three-Dimensional Mode

The term "three-dimensional" here refers to the fact that the bank-angle magnitude and sign are both defined in the parameterization, and the corresponding trajectory covers both longitudinal and lateral motions. Two parameters are used to define the bank-angle profile $\sigma(\cdot)$, which is the minimum number required to explicitly meet the two terminal constraints in Eq. (11). The algorithm plans for a single bank reversal in which the sign of the bank angle begins to change. To maintain the same 2 degrees of freedom in the bank profile after the bank reversal, we choose two different forms of parameterization before and after the bank reversal.

A. Prereversal Phase

This is the phase before the vehicle has executed the bank reversal. In this phase, the magnitude of the bank angle is defined in the same fashion as in Eq. (24), with σ_0 as the parameter to be determined. In comparison, a constant bank magnitude profile is used in Fuhry [4] and Kaluzhskikh and Sikharulidze [5]. The benefits of the enhanced robustness of the profile in Eq. (24) as discussed in Sec. III.B motivates our current choice. As such, we may call this formulation *robustified 3-D mode*, and the parameterization with a constant bank magnitude *baseline 3-D mode*. Indeed, our tests show visible improvements in dispersed simulations with this robustification in the bank-angle profile over the baseline mode as in the existing literature (see Sec. VI.D). The second parameter is e_1, the energy at which the bank reversal begins. During the bank reversal, the bank

angle moves at the maximum allowable rate to the negative of $\sigma(e_1)$. The initial sign of the bank angle is chosen to be the opposite of that of the initial cross range so as to reduce the cross range. The profile in the solid line in Fig. 1 illustrates the complete bank-angle history in the prereversal phase.

For any given pair $\{\sigma_0, e_1\}$, the trajectory can be propagated to the specified final energy e_f by numerically integrating Eqs. (9), and the terminal longitude θ_f and latitude ϕ_f are determined. In this sense, the final longitude and latitude are functions of $\{\sigma_0, e_1\}$ (albeit through numerical integration). Consequently, the satisfaction of the two terminal constraints in Eq. (11) can be regarded as a root-finding problem in which the following two nonlinear algebraic equations are to be solved:

$$F_1(\sigma_0, e_1) = \theta_f(\sigma_0, e_1) - \Theta^* = 0 \qquad (25)$$

$$F_2(\sigma_0, e_1) = \phi_f(\sigma_0, e_1) - \Phi^* = 0 \qquad (26)$$

The classical Newton–Raphson method for finding the zero of nonlinear algebraic systems can be employed for finding the solution (σ_0, e_1). The gradients of F_1 and F_2 are found by forward finite difference. Thus each Newton iteration involves integrating the system equation (9) from e_0 to e_f three times.

B. Postreversal Phase

After the trajectory has passed the planned bank reversal, the parameterization of the bank-angle profile in prereversal mode is no longer applicable because no bank reversal is planned anymore. Hence, the problem loses 1 degree of freedom (the one defining the bank-reversal point) after the trajectory passes the bank reversal. The algorithm in Fuhry [4] switches after the bank reversal to search for the constant bank-angle magnitude to minimize the miss distance to the landing site (thus, it becomes a one-parameter problem). The potential problem is that the miss distance could still be large because the polarity of the bank angle is fixed, and corrections on the cross range may not be fully achieved. Realizing the potential drawbacks due to the loss of lateral control after the bank reversal, the approach in Kaluzhskikh and Sikharulidze [5] employs a (somewhat cumbersome) logic in an attempt to push the designed bank reversal closer to the landing site.

In our approach, we will continue to use the energy-dependent profile in Eq. (24) to define the bank angle. The difference is that both parameters σ_0 and σ_f are now to be determined (including their signs and magnitudes). To distinguish this variable value of the final bank angle from the specified value in Eq. (24), it is designated as σ_2 in the postreversal phase, and the dashed line in Fig. 1 illustrates the postreversal bank-angle parameterization. Therefore, we still have a two-parameter parameterization in the postreversal phase. These two parameters are allowed to have different signs, thus permitting a possible change of the sign of the bank angle in this phase, if necessary. This option is intentionally kept to preserve the algorithm's ability to counter trajectory dispersions and modeling uncertainties. Using the aforementioned reasoning, the final longitude and latitude can again be considered functions of σ_0 and σ_2. Hence, the miss-distance functions F_1 and F_2 in Eqs. (25) and (26) are now functions of ($\sigma_0 \quad \sigma 2$). The same process can be used to
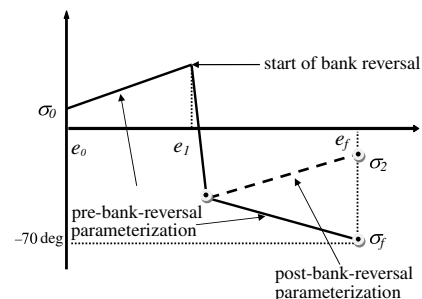

Fig. 1 **Parameterization of the bank-angle profile in 3-D mode.**

find σ_0 and σ_2. Therefore, the only difference between the prereversal and postreversal phases lies in the parameterization of the bank-angle profile. The number of parameters and the algorithm are all the same.

In principle, the same linear bank-angle profile may be used throughout the entry flight as it is applicable whether or not the sign of the bank angle needs a change. But it is not desirable to use the linear parameterization early in the trajectory because the signs of σ_0 and σ_2 are bound to be different in such a case. The restrictive *linear* profile over a long flight time will cause the bank angle to have a small magnitude for a considerable duration (around the zero-crossing point). The result is that the initial and final bank angle will have to be quite large to dissipate the fixed amount of energy. Such a trajectory could suffer from unnecessarily high load and heating.

V. Predictive Load Relief

For a crewed vehicle, it is crucial that the load-factor constraint along the entry trajectory is not grossly violated. This constraint can be in the simplest form in which the load factor should be no greater than a specified value:

$$n_a = \sqrt{L^2 + D^2} \leq g_{\max} \qquad (27)$$

More elaborate forms of the constraint can be defined by different plateau times for the load factor to exceed different threshold values. We will use the form in Eq. (27) in our discussion. The guidance solution of the predictor-corrector algorithm does not explicitly enforce such a constraint. Certain reactive measures may be taken outside of the predictor-corrector algorithm to attempt to relieve the load in the case in which the load factor exceeds the limit. In Braun and Powell [2], the commanded bank angle is set to zero whenever the load limit is violated. A slightly more elaborate, yet essentially similar, approach called the g limiter is taken in the Apollo guidance [9]. Alternatively, one can compute the bank-angle command needed to fly a constant load factor (at the limit) directly from the equations of motion and use it instead whenever the load exceeds the limit. For our applications, these approaches are found in many cases to cause an unacceptable degradation in landing precision when the overshoot over the load limit is substantial. This is because, for low-lifting entry vehicles, the remaining time to go is relatively short after the trajectory exits the high-g region. The interruption in steering the vehicle toward the landing site caused by such a reactive load-relief maneuver tends to create large trajectory dispersions from which the vehicle cannot recover in the short time remaining.

The incorporation of the enforcement of the load-factor constraint directly in the predictor-corrector algorithm will significantly complicate the algorithm and adversely affect the convergence of the algorithm. Instead, we will take advantage of the feature that a predicted peak load factor is readily available from the trajectory produced by the predictor-corrector algorithm and propose a load-relief approach that appears to be effective for low-lifting entry vehicles.

For entry missions from orbit, such as International Space Station (ISS) return missions, the entry interface (EI) is traditionally set at the altitude of 121.92 km (400,000 ft). But the closed-loop guidance will not be initiated until the drag acceleration reaches a certain level (0.2 g in Apollo final-phase entry guidance), which is typically at about 80 km in altitude. During the initial descent between 121.92 km and 80 km, the vehicle flies open loop. Choosing an appropriate constant bank angle for the vehicle during this period proves to be an effective means to lower the peak load factor. Figure 2 shows the closed-loop bank-angle profiles under the predictor-corrector guidance and the corresponding load-factor variations for a capsule vehicle along three trajectories. The entry condition and landing site are identical for all three trajectories. The only difference lies in the constant bank angle flown during the initial descent at 0, -90, and -180 deg, respectively. The dramatic influence of these different initial bank angles is evident from the second plot of Fig. 2, in which the peak load factor is reduced from 7.8 to 4.2 g.

At first glance, it may seem counterintuitive that flying a larger initial bank angle actually reduces the peak load factor. Figure 3
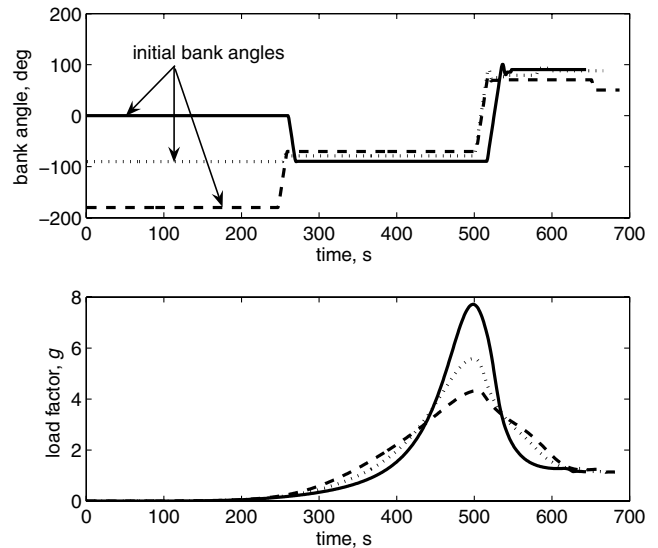

Fig. 2 Effects of using different bank angles in the initial open-loop descent on reducing the peak load factor.
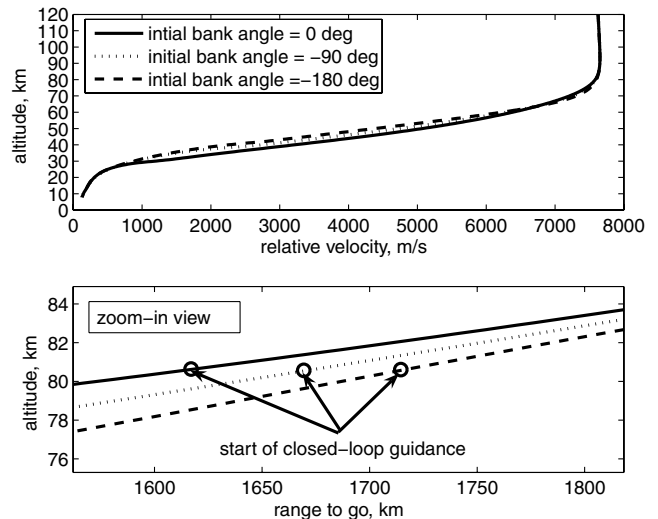

Fig. 3 Effects of different bank angles in the initial descent on trajectory.

reveals the reason. The first plot of Fig. 3 shows that, as the magnitude of the initial bank angle increases, the later part of the trajectory becomes more lofted. This lofting directly contributes to the lower peak load factor. The reason for the different altitude profiles is answered in the second plot of Fig. 3. As the lift vector is pointed more and more downward as the magnitude of the bank angle is increased in the initial descent, the range to go at the initiation of the closed-loop guidance becomes longer. To cover a longer range with approximately the same energy, the vehicle will have to fly a more lofted trajectory. Note that, even though the range differences shown in the second plot of Fig. 3 are only about 100 km at most, they are enough to cause considerable differences in the subsequent parts of the trajectories. This is just another manifestation of the low L/D of the vehicle. This phenomenon is also tied to the use of predictor-corrector guidance. If the entry guidance is based on the tracking of a fixed reference profile, as in the Apollo guidance, such a trend will probably be much less definitive. For vehicles with moderate to higher L/D ratios, this phenomenon may not be as clear, and other approaches are more effective at enforcing the path constraints [8,10].

The preceding observations made on the basis of Figs. 2 and 3 lead to the following load-relief strategy, in conjunction with the use of

the predictor-corrector guidance, that can be executed onboard at the entry interface:

1) Starting from the actual EI condition, the trajectory is propagated with a nominal constant bank angle, $\sigma_0 = 0$ deg, to the altitude at which the drag acceleration reaches 0.2 g. The predictor-corrector entry guidance algorithm is called from that condition to generate a trajectory to the landing site. The corresponding peak load factor $n_{a_{\max}}^{(1)}$ is checked to see if it exceeds the limit $g_{\max}$. If not, the initial descent phase is continued with this nominal bank angle until the initiation of closed-loop guidance; otherwise, go to the next step.

2) The initial magnitude of the bank angle is increased at a given increment to be $|\sigma_0| = 90$ deg, and the same process as in step 1 is repeated to obtain the new predicted peak load factor $n_{a_{\max}}^{(2)}$. If $n_{a_{\max}}^{(2)} \leq g_{\max}$, the initial bank-angle magnitude is set at 90 deg and this initial selection logic is completed; if $n_{a_{\max}}^{(2)} > g_{\max}$ still, go to step 3.

3) The initial bank angle, $\sigma_0 = 180$ deg, will be used.

After the initial bank-angle magnitude is determined, the initial descent is flown with it and the sign of the bank angle is set in the direction of reducing the initial cross range. At the activation of closed-loop guidance, the predictor-corrector guidance algorithm takes over. Note that so far it is deliberate not to explicitly state which mode of the predictor-corrector algorithm (in Sec. III or IV) will be used. Either mode in principle is applicable. Because the longitudinal mode as presented in Sec. III.B will be demonstrated to be more robust for guidance, it will be the likely choice.

The aforementioned strategy may be further fine tuned, if needed, but the same principle remains. This strategy ensures that, within the feasibility of the trajectory, the violations of the load-factor constraint, if any, would not be as severe. And in such a case, the application of additional load-relief maneuvers as in Braun and Powell [2] and Moseley [9] will stand a much improved chance of success. Note that indiscriminately flying a large bank angle during the initial descent, regardless of whether it is needed for load relief, is not advisable because doing so could unnecessarily reduce the energy margin in some cases. The preceding strategy is designed to do that only in the case of necessity in which the peak load factor must be lowered.

It should be mentioned that, because the peak heating rate always occurs considerably earlier than the peak load factor [11], the aforementioned strategy does not appear to significantly reduce the peak heating rate as it does the peak load factor. In fact, in the subcircular entry flight of low-lifting entry vehicles, the peak heating rate is largely determined by the entry condition. Thus, it is much more effective to control the entry condition to achieve an acceptable peak heating rate.

VI. Simulation Evaluation and Discussion

A. Vehicle Model

The entry vehicle model used in the simulations is that of a capsule vehicle, shown in Fig. 4. The vehicle is similar in size, weight, and aerodynamic characteristics to the Orion CEV. The base of the vehicle has a diameter of 5 m. The mass of the vehicle is 8383 kg (18,464 lb). At Mach 25, the vehicle flies a trim angle of attack of about 160.3 deg, which results in a L/D of 0.2877. The trim angle of attack is a function Mach number, thus the L/D varies between 0.223 and 0.407 along the trajectory, with the maximum L/D occurring at Mach 1.52. The maximum bank rate of the vehicle is limited at 20 deg/s and the maximum bank acceleration at 10 deg/s^2.

B. Three-Degree-of-Freedom Dispersion Simulation Setup

The EI is defined by the altitude of 121.92 km (400,000 ft). The nominal entry conditions at the EI correspond to those of an ISS orbit return mission landing at Edwards Air Force Base (EAFB). The end of the entry flight, that is, the drogue deployment, is at a terminal energy corresponding to nominally 7.62 km (25,000 ft) in altitude and at a relative velocity of 150 m/s. Figure 5 shows the nominal bank-angle profiles and trajectories under guidance by the
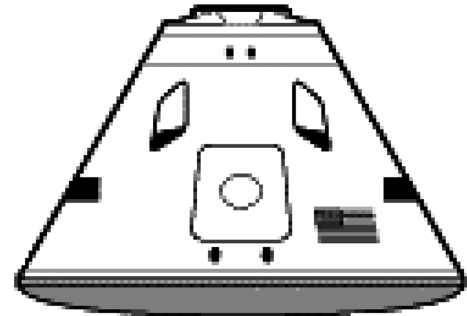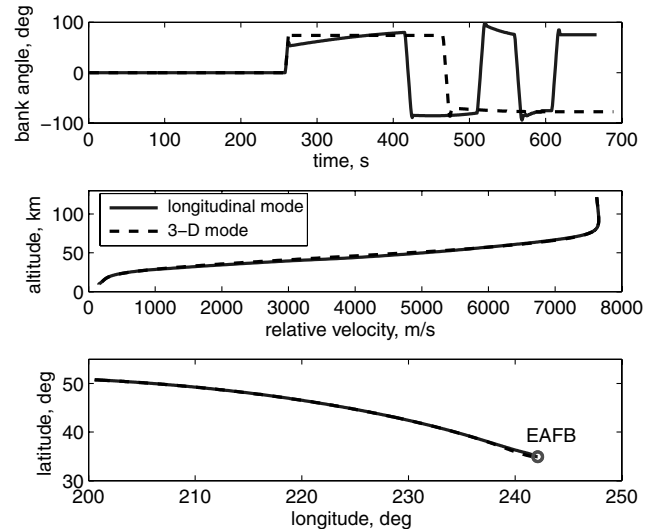

Fig. 4   Capsule entry vehicle.

Fig. 5   Nominal trajectory profiles for an ISS return mission landing at EAFB.

robustified longitudinal and 3-D modes of the predictor-corrector algorithm, respectively.

The dispersed entry conditions at the EI are related to the dispersions in the position and relative velocity at the deorbit-burn point by a covariance matrix. The random dispersions in the three position vector components are assumed to be in zero-mean Gaussian distributions with a 3-σ value of 30 m. The dispersions in the velocity components are in zero-mean Gaussian distributions with a 3-σ value of 0.3 m/s. Through the covariance matrix, these values produce the 3-σ EI condition dispersions summarized in Table 1. Compared with the EI condition dispersions used in a recent work on Orion CEV [12], the dispersions used here in longitude and latitude are about three times larger and eight times larger in heading angle; the dispersions in the flight-path angle are about $\frac{1}{4}$ compared with those in Rea and Putnam [12]. The dispersions in the other key parameters are also listed in Table 1.

Uniformly distributed random biases to C_L and C_D are added to the nominal values in the simulations. Typically, zero-mean

Table 1   Dispersions in the entry interface state and other parameters

State/parameter	Distribution	3-σ value/range
Longitude, deg	Zero-mean Gaussian	0.59
Latitude, deg	Zero-mean Gaussian	0.66
Relative velocity, m/s	Zero-mean Gaussian	0.41
Flight-path angle, deg	Zero-mean Gaussian	0.023
Heading angle, deg	Zero-mean Gaussian	0.39
C_L	Uniform	±0.03
C_D	Uniform	±0.06
Mass, kg	Uniform	±5%
Atmospheric density	Uniform	±30%

Gaussian distributions are used for dispersions in C_L and C_D. Uniform dispersions are considerably more stressful than zero-mean Gaussian dispersions with a 3-σ value of the same magnitude as the range of the uniform distribution. For atmospheric dispersions, ideally the GRAM99 model [13] should be used for the testing. Without access to GRAM99 at the time of this work, a simple atmospheric density dispersion model was used in the simulations:

$$\rho = [1 + \Delta_{\text{atmsph}} + \Lambda_{\text{atmsph}} \sin(\omega h + \varphi_0)]\rho_{\text{ref}} \qquad (28)$$

where ρ_{ref} is the atmospheric density from the 1976 U.S. Standard Atmosphere. Δ_{atmsph} and Λ_{atmsph} are two uniformly distributed random numbers in the range of ± 0.15. The quantity of $\omega > 0$ and φ_0 are two fixed constants, and h is the altitude. This simple model attempts to capture some of the known characteristics of the dispersions in the atmospheric density in both biased and altitude-dependent fashions [14]. The performance of the current predictor-corrector guidance algorithm under more elaborate atmospheric density dispersions can be found in Brunner and Lu [15].

In the 3-DOF trajectory simulations, the equations of motion, Eqs. (1–6), are used, with all the dispersions listed in Table 1 added. For the trajectory propagations in the predictor-corrector algorithm, Eqs. (1–6) with nominal vehicle parameters and a nominal atmospheric model are used in all of the cases except for the baseline longitudinal mode. In the longitudinal baseline mode, the reduced longitudinal equations, Eqs. (14–17), are integrated for trajectory propagation in the guidance algorithm.

The landing precision requirement is within 5 km of the landing site for the Orion program. Because adequate margins should be left for a 6-DOF flight and parachute descent, a dispersed 3-DOF simulation is considered a successful run when the final position of the vehicle is within 2.5 km of the landing site. If the final position is outside the 2.5-km radius but within a 5-km radius circle, it is judged to be a 50% success. Any 3-DOF trajectory ending outside of the 5-km radius of the landing site is regarded as a failure. It should be noted that navigation uncertainties are not considered here. The testing results should be viewed in this context. However, it is well recognized that the uncertainties of state-of-the-art navigation systems are not primary factors affecting the precision of the entry guidance system.

C. Effectiveness of Load-Relief Strategy

The first item of testing is the load-relief strategy in Sec. V. The maximum peak load factor in constraint (27) is set at $g_{\max} = 4.5$ g. The longitudinal predictor-corrector algorithm described in Sec. III.B is used for both load-relief prediction and closed-loop guidance after the aerodynamic load exceeds 0.2 g. The variations of the load factor along 500 dispersed trajectories are shown in the first plot of Fig. 6. In comparison, the same 500 dispersed cases are also simulated without employing the load-relief strategy (zero bank angle during the initial descent from the EI), but still with the same closed-loop predictor-corrector guidance. The second plot in Fig. 6
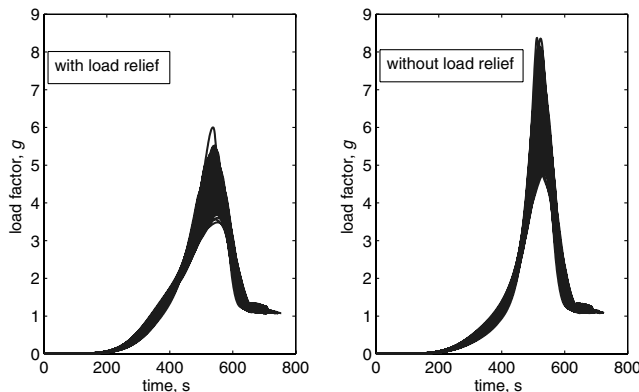
Table 2 Statistics on the peak load factor for 500 trajectories in Fig. 6

Peak load factor, g	With load relief ($g_{\max} = 4.5$ g)	Without load relief
Average	4.4981	6.2402
Median	4.4685	6.1392
Maximum	6.0007	8.3772
Minimum	3.4848	4.7615
Standard deviation	0.3960	0.6827

illustrates the histories of the load factor along these trajectories. It is immediately evident that the load-relief strategy in general lowers the peak load factor considerably. The statistics on the values of the peak load factor in Table 2 give more quantitative measures. The average value of the peak load factor is 4.498 g (very close to $g_{\max} = 4.5$ g) with the load-relief strategy implemented, as opposed to an average of 6.24 g without. The data in Table 2 clearly confirm the effectiveness of this simple, yet well-founded, strategy. In the cases in which the peak load factor still exceeds the 4.5 g limit even with this strategy, the reasons are threefold: 1) the initial condition is such that even with 180 deg initial bank angle, the peak load factor cannot be lowered below 4.5 g; 2) the dispersions in the aerodynamic coefficients, mass, and up to 30% variations in the atmospheric density cause a higher load factor, which the predictor-corrector algorithm cannot predict based on the nominal models; and 3) the combination of 1 and 2.

All of the dispersed trajectories shown in Fig. 6 landed within 2.5 km of the intended landing site at EAFB. More on landing precision is given in the next section.

D. Landing Precision and Comparison

The performance of the entry guidance algorithm is ultimately judged by how accurately it can guide the vehicle to the landing site in the presence of substantial uncertainties and dispersions. When the robustified longitudinal predictor-corrector algorithm described in Sec. III.B is used in the closed-loop guidance for the 500 cases, all of the trajectories land within 2.5 km of the landing site at EAFB. The final positions of the trajectories around the landing site are shown in squares in Fig. 7, and the statistics of the miss distances are summarized in Table 3. The final positions of the trajectories are tightly clustered around the landing site, with an average miss distance of 0.945 km and a standard deviation of 0.353 km. To appreciate how much the robustification measure in Eq. (24) enhances the overall performance of the algorithm, the baseline longitudinal algorithm in Sec. III.A is also applied to the same 500 dispersed cases for comparison. The final positions under the baseline algorithm are also plotted in Fig. 7 in circles, and the
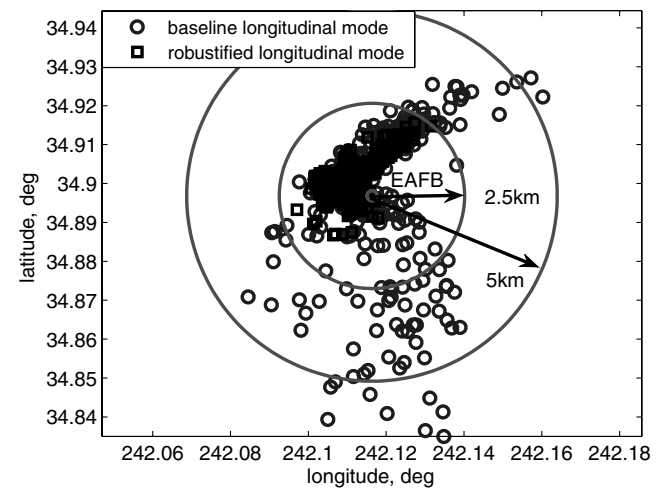

Fig. 7 Final positions around the landing site in 3-DOF dispersion simulations, guided, respectively, by the robustified (squares) and baseline (circles) *longitudinal mode* of the predictor-corrector algorithm (the same 500 cases each).

Fig. 6 Load-factor variations along 500 dispersed trajectories with and without implementing the load-relief strategy ($g_{\max} = 4.5$ g).
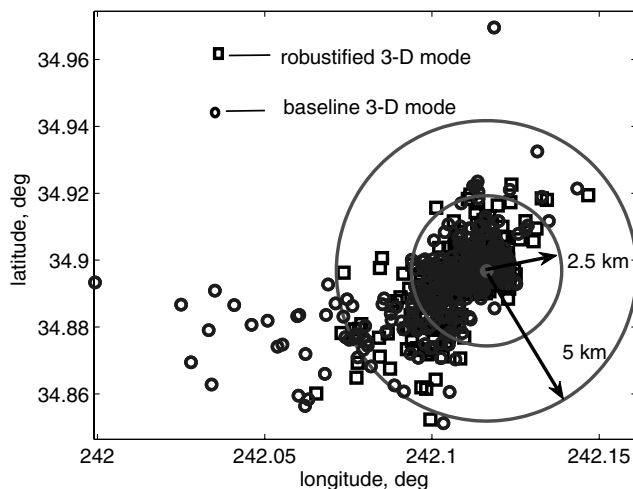
Table 3 Statistics on the final miss distances in 500 dispersed trajectories under longitudinal predictor-corrector guidance, with dispersions listed in Table 1

Miss distance, km	Baseline longitudinal mode	Robustified longitudinal mode
Average	1.478	0.945
Median	1.111	0.893
Maximum	7.092	2.443
Minimum	0.018	0.051
Standard deviation	1.240	0.353

statistics of miss distances are listed in Table 3 as well. The comparison seen in Fig. 7 is telling: with an average miss distance already at 1.478 km and a large standard deviation of 1.24 km, quite a few of the trajectories end outside of the 2.5-km circle and some outside the 5-km circle. The baseline longitudinal predictor-corrector algorithm would have difficulty meeting the stringent landing precision requirements.

Next, the 3-D mode of the predictor-corrector guidance algorithm presented in Sec. IV is employed in the same 500 dispersed simulations. Again, both the baseline and robustified 3-D modes are tested. Figure 8 shows the scattering of the final positions of the entry trajectories and Table 4 summarizes the statistics of the miss distances. It is clear from Fig. 8 that the robustified bank-angle profile in Eq. (24) also visibly improves the performance in 3-D mode as compared with the baseline of constant bank-angle parameterization. However, in contrast with the results seen in Fig. 7 and Table 3, even the performance of the robustified 3-D mode does not come close to that of the robustified longitudinal mode in terms of meeting the landing precision requirement in a statistical sense (in fact, the performance of the robustified 3-D mode is comparable to that of the baseline longitudinal mode as seen in Fig. 7 and Table 3). This conclusion turns out to be true in all of the dispersion tests we conducted, even though only a small fraction of the results is reported here.

In the case in which the 3-D mode of the guidance algorithm ends with a large miss distance, it is inevitably because the algorithm encounters convergence difficulty in the postreversal phase. This happens when large uncertainties exist in the aerodynamic or atmospheric models. In the case of nonconvergence, the algorithm cannot find the two parameters σ_0 and σ_2 as shown in Fig. 1 to simultaneously satisfy the end conditions in Eq. (11). The underlying reason, however, is related to an inherent characteristic in the trajectory with the single reversal structure of the bank angle in Fig. 1. With just *one* bank reversal planned, the cross range of the trajectory will be at near maximum right before the bank reversal, which typically takes places relatively far from the landing site.

Table 4 Statistics on the final miss distances in 500 dispersed trajectories under the 3-D mode of predictor-corrector guidance

Miss distance, km	Baseline 3-D mode	Robustified 3-D mode
Average	1.287	1.002
Median	0.635	0.616
Maximum	10.715	6.197
Minimum	0.001	0.005
Standard deviation	1.574	1.0

When the dispersions are such that the actual L/D is substantially lower than its nominal value, which is used to plan the trajectory by the algorithm, the vehicle could experience difficulties nulling the cross-range error and still meet the downrange requirement. A possible remedy is to push the planned bank reversal closer to the landing site, for instance, by first using the Apollo type of lateral logic to command a few bank reversals earlier in the trajectory. Of course, care must be exercised to make sure that, after these bank reversals, a bank-reversal opportunity still remains for the algorithm to plan. Conceivably, such an added logic will only increase the complexity of the algorithm.

The longitudinal mode does not suffer from this problem, because the lateral bank-reversal logic always reactively limits the cross range within a corridor.

E. Doubling Aerodynamic Uncertainty

The strong robustness of the robustified longitudinal predictor-corrector guidance algorithm is further demonstrated by increasing the aerodynamic modeling uncertainty. Now let us double the aerodynamic uncertainty in Table 1 by allowing up to ± 0.12 in the dispersions in C_D and ± 0.06 in C_L. These values amount to

Fig. 8 Final positions around the landing site in 3-DOF dispersion simulations, guided, respectively, by the robustified (squares) and baseline (circles) *3-D mode* of the predictor-corrector algorithm (the same 500 cases each).
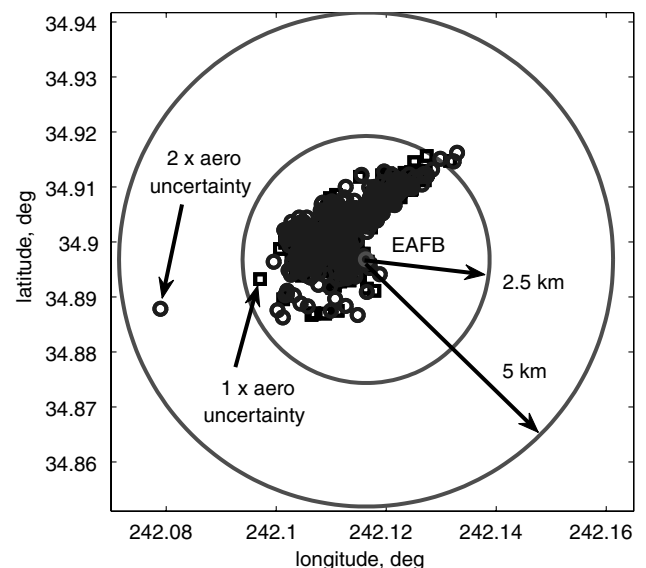

Fig. 9 Final positions in 500 3-DOF dispersion simulations with an aerodynamic uncertainty twice the values in Table 1 (circles) and the same 500 cases with the aerodynamic uncertainty listed in Table 1 (squares) under robustified longitudinal predictor-corrector guidance.

Table 5 Statistics on the final miss distances in 500 dispersed trajectories with a 100% increase in the dispersions in C_D and C_L under robustified longitudinal predictor-corrector guidance

Miss distance statistics	Value, km
Average	0.959
Median	0.909
Maximum	3.568
Minimum	0.074
Standard deviation	0.401

approximately 30% dispersions in L/D (20% in C_L and 10% in C_D). The otherwise same 500 cases are simulated again. Table 5 lists the final precision statistics. Compared with the data for the robustified longitudinal predictor-corrector guidance in Table 3, we see a virtually identical performance, despite the increase of the aerodynamic uncertainty by 100%. Figure 9 depicts the scattering of the final positions along the 500 trajectories. For the convenience of comparison, the final positions before the doubling of the aerodynamic uncertainty are also plotted in Fig. 9 in squares (the same ones as in Fig. 7). In nearly every case, the final position of the trajectory is almost the same despite the 100% increase in aerodynamic uncertainty. The most visible exception is the one case in which the final miss distance is now 3.57 km, whereas before it was within 2.5 km of the landing site. Such consistent performance of the longitudinal predictor-corrector guidance algorithm developed here instills much confidence in the algorithm for potential onboard applications.

The applications and performance of the robustified longitudinal predictor-corrector entry guidance algorithm in the final phase of skip entry flight for lunar-return missions can be found in Brunner and Lu [15].

VII. Conclusions

The predictor-corrector approach discussed in this paper holds strong potential for robust and accurate entry guidance for vehicles with low lift-to-drag ratios. The new design features developed here for the enhancement of robustness in the bank-angle parameterization prove to be essential to the success of the algorithm in severely dispersed cases. Under the predictor-corrector guidance, the peak load factor along the entry trajectory of a low-lifting vehicle is found to be correlated inversely with the magnitude of the bank angle in the initial decent. A predictive load-relief strategy using the predictor-corrector algorithm in an open-loop fashion appears effective and overcomes a major shortcoming of the existing reactive approaches that tends to interfere with and compromise the guidance precision. Among the two popular forms of bank-angle parameterization examined, our testing results clearly show that the robustified longitudinal predictor-corrector algorithm is suitable for closed-loop entry guidance applications, given its consistently strong performance and robustness. On the other hand, the 3-D version is less robust in the presence of severe modeling uncertainties. The root cause lies in the single bank-reversal structure of the bank-angle parameterization. The discussions on various aspects of entry flight and guidance of low-lifting vehicles throughout the paper should provide useful insight into vehicle design and mission planning.

References

[1] Gamble, J. D., Cerimele, C. J., Moore, T. E., and Higgins, J., "Atmospheric Guidance Concepts for an Aeroassisted Flight Experiment," *Journal of Astronautical Sciences*, Vol. 36, No. 1, 1988, pp. 45–71.

[2] Braun, R. D., and Powell, R. W., "Predictor-Corrector Guidance Algorithm for Use in High-Energy Aerobraking System Studies," *Journal of Guidance, Control, and Dynamics*, Vol. 15, No. 3, 1992, pp. 672–678.

[3] Powell, R. W., "Six-Degree-of-Freedom Guidance and Control-Entry Analysis for HL-20," *Journal of Spacecraft and Rockets*, Vol. 30, No. 5, 1993, pp. 537–542.

[4] Fuhry, D. P., "Adaptive Atmospherics Reentry Guidance for the Kistler K-1 Orbital Vehicle," AIAA Paper 99-4211, Aug. 1999.

[5] Kaluzhskikh, Y. N., and Sikharulidze, Y. G., "A Control Algorithm for Reentry of a Rescue Space Vehicle into the Earth's Atmosphere," *Cosmic Research (Translation of Kosmicheskie Issledovaniya)*, Vol. 38, No. 3, 2000, pp. 262–269.

[6] Zimmerman, C., Dukeman, G., and Hanson, J., "Automated Method to Compute Orbital Reentry Trajectories with Heating Constraints," *Journal of Guidance, Control, and Dynamics*, Vol. 26, No. 4, 2003, pp. 523–529.

[7] Putnam, Z. R., Braun, R. D., Bairstow, S. H., and Barton, G. H., "Improving Lunar Return Entry Footprint Using Enhanced Skip Trajectory Guidance," AIAA Paper 2006-7438, Sept. 2006.

[8] Harpold, J. C., and Graves, C. A., "Shuttle Entry Guidance," *Journal of Astronautical Sciences*, Vol. 37, No. 3, 1979, pp. 239–268.

[9] Moseley, P. E., "The Apollo Entry Guidance: A Review of the Mathematical Development and Its Operational Characteristics," TRW, 69-FMT-791, Houston, TX, Dec. 1969

[10] Shen, Z., and Lu, P., "On-Board Generation of Three-Dimensional Constrained Entry Trajectories," *Journal of Guidance, Control, and Dynamics*, Vol. 26, No. 1, 2003, pp. 111–121.

[11] Lu, P., and Vinh, N. X., "Minimax Optimal Control for Atmospheric Fly-Through Trajectories," *Journal of Optimization Theory and Applications*, Vol. 57, No. 1, 1988, pp. 41–58. doi:10.1007/BF00939328

[12] Rea, J. R., and Putnam, Z. R., "A Comparison of Two Orion Skip Entry Guidance Algorithms," AIAA Paper 2007-6424, Aug. 2007.

[13] Justus, C. G., and Johnson, D. L., "The NASA/MSFC Global Reference Atmospheric Model—1999 Version (GRAM-99)," NASA TM-1999-209630, 1999.

[14] Findlay, J. T., Kelly, G. M., McConnell, J. G., and Compton, H. R., "Shuttle 'Challenger' Aerodynamic Performance from Flight Data Comparisons with Predicted Values and 'Columbia' Experience," AIAA Paper 84-0485, Jan. 1984.

[15] Brunner, C. W., and Lu, P., "Skip Trajectory Planning and Guidance," AIAA Paper 2007-6777, Aug. 2007.